Journal of Food Engineering 118 (2013) 256–265

Contents lists available at SciVerse ScienceDirect

Journal of Food Engineering

journal homepage: www.elsevier.com/locate/jfoodeng

Effect of mixer geometry and operating conditions on mixing efficiency of a non-Newtonian fluid in a twin screw mixer

Maureen L. Rathod [a], Jozef L. Kokini [a,b,*]

[a] Department of Food Science, Rutgers University, New Brunswick, NJ 08901, United States
[b] Department of Food Science and Human Nutrition, University of Illinois at Urbana Champaign, Urbana, IL 61801, United States

ARTICLE INFO

Article history:
Received 11 July 2012
Received in revised form 24 March 2013
Accepted 19 April 2013
Available online 30 April 2013

Keywords:
Non-Newtonian fluid
Numerical simulation
Twin-screw mixer

ABSTRACT

The effect of mixer speed, fluid inflow rate, and paddle angle was examined in a shortened geometry. 3D FEM simulation of non-Newtonian 2 g/100 mL carboxymethyl cellulose aqueous solution in the mixing region of a Readco continuous mixer was performed. Data gathered included velocity vectors, shear rate, and mixing index. Increasing mixer speed increased velocity magnitudes in the horizontal and vertical directions. Fluid inflow rate had little impact on velocity in the horizontal and vertical directions, but increased velocity in the axial direction and elongational contribution to the mixing index. All configurations showed areas of simple shear flow where the fluid experienced high shear rates. Staggering paddles increased the maximum axial velocity and shear rate. When successive paddles on the same screw are parallel, a zone was seen between the center of the paddle and the barrel wall which demonstrated efficient dispersive mixing.

1. Introduction

Mixing is an important process in the production of foods, polymers, and pharmaceuticals. It is used to blend different components, to develop desirable product attributes and to introduce air. All of these processes are important to mixing of wheat flour with water and other ingredients resulting in wheat flour doughs. In this system, water must be distributed and flour particles must be broken to release starch and protein to allow gluten formation. Additionally, mixing is used to stretch glutenin promoting molecular alignment and the formation of non-covalent bonds giving dough elasticity, imparting machinability and gas retention. Bubbles introduced during mixing become nuclei for carbon dioxide formed in fermentation and allow for expansion of the dough during proofing (Connelly and Kokini, 2007).

Various kinds of mixers promote different types of mixing. These include batch and continuous mixers and those with both fixed and variable geometries. Effective mixers often have complex geometries and several moving parts. Numerical simulation can provide velocity, shear rate, shear stress, temperature, and moisture content distribution within the mixer in a non-destructive manner which is a distinct advantage over experimental measurements that often disturb the fluid while acquiring data. One major limitation of numerical simulation is the increased computational requirement for more complicated simulations. Using a more complex mixer geometry and fluid increases the equipment and time cost, especially when the fluids being mixed are very viscous or viscoelastic.

In determining mixing efficiency, one can examine both dispersive and distributive mixing. Distributive mixing spreads particles throughout the mixer volume and is influenced by fluid stretching and reorientation. Measures of distributive mixing include length of stretch, stretching efficiency, and segregation scale. Dispersive mixing separates clumps or aggregates in the mixer through shear and elongational stresses (Alsteens et al., 2004). It is measured by the Manas-Zloczower mixing index.

Muzzio and his research group (Alvarez et al., 2002; Lamberto et al., 2001; Zalc et al., 2001; Portillo et al., 2008, 2009) have studied stirred tank reactors, static mixing flows, and mixing in laminar to turbulent flow regimes with generalized Newtonian fluids. These investigations have involved experimental and computational fluid dynamics (CFD) work. Lamberto et al. (2001) used a rotating reference frame technique to examine laminar mixing of a Newtonian fluid in an unbaffled stirred tank with an impeller. This study was comparable to simulations performed using a classical geometry and varying time-periodic boundary conditions. The objective was to observe the effect of varying speed on mixing performance. They found the toroidal structures which form at a constant impeller speed periodically relocated if the speed varied between two values. This relocation caused an exponential increase in stretching. Increasing the frequency of the speed fluctuation also increased the stretching rate. Simulation results were a close match to data obtained by particle image velocimetry (PIV) in a seeded glycerin solution.

* Corresponding author at: Department of Food Science, Rutgers University, New Brunswick, NJ 08901, United States.
E-mail addresses: kokini@illinois.edu, jkokini51@gmail.com (J.L. Kokini).

0260-8774/$ - see front matter © 2013 Elsevier Ltd. All rights reserved.
http://dx.doi.org/10.1016/j.jfoodeng.2013.04.020

Nomenclature

v_x	velocity in the x direction (horizontal)	n	power-law index
v_y	velocity in the y direction (vertical)	λ_{MZ}	Manas-Zloczower mixing index
v_z	velocity in the z direction (axial)	$\boldsymbol{\Omega}$	vorticity tensor
$\mathbf{T}$	extra stress tensor	H	step function
$\mathbf{D}$	rate of deformation tensor	$\mathbf{v}$	velocity
η	dynamic viscosity	$\bar{\mathbf{v}}$	local moving part velocity
T	temperature	$\mathbf{a}$	acceleration
$\dot{\gamma}$	local shear rate	p	pressure
K	consistency factor	ρ	density
t	natural time	β	compression factor

More recently, Portillo et al. (2008) examined the mixing of acetaminophen and lactose in a continuous convective blender. Their goal was to see the effect of blade design, mixer rotation rate, and processing angle on mixing efficiency. Blended samples were taken at the blender outlet and analyzed using NIR to determine their composition. Relative standard deviation (RSD) of tracer concentration was used as a measure of homogeneity. Lower RSD was taken as an indicator of less sample variability and therefore better mixing. The variance reduction ratio (VRR) which is the ratio of the calculated variance for the material entering and exiting the mixer measures the ability of a mixer to eliminate variability found in the product before entering the mixer. The upward processing angle (where the exit of the mixer was positioned higher than the entrance) resulted in the largest mean residence time as well as the lowest RSD and highest VRR providing the best mixing performance. Increasing mixer rpm decreased the powder residence time but increased the number of blade passes it experienced resulting in more variability with increasing speed. Increasing the blade angle from 15° to 60° decreased the RSD, but above 60° the axial transport was not strong enough to continue the trend.

In comparing different blenders, Portillo et al. (2009) found that the effectiveness of a mixer was affected by the design of the impeller and blades. The blade angle relative to the shaft affected mixing performance Impeller rotation rate caused the most significant effect on relative variance, followed by powder cohesion, and then vessel angle. Rotation rate and processing angle significantly affected residence time, with rotation rate having a greater influence. A direct correlation was found between improved mixing and higher residence time.

Zhang et al. (2009) examined residence time distribution (RTD) of a co-rotating twin screw extruder using CFD and compared the data obtained with experimental results. They analyzed the distributive mixing performance of different kneading disc types by measuring the area stretch ratio, instantaneous efficiency and time-averaged efficiency. The researchers found that local RTD was affected by both operating conditions (screw speed and feed rate) and the geometry of the kneading discs used. Mean RTD increased while axial mixing decreased with increasing stagger angle of the kneading discs. Generally, kneading discs with a disc gap, small disc width, and large stagger angle produce good distributive mixing performance.

Previous numerical simulation work has frequently examined mixing behavior of simple fluid in simplified geometries. In our lab, geometries resembling those in industrial mixers have been used with Newtonian and non-Newtonian fluids (Connelly and Kokini, 2003, 2004, 2006a, 2006b, 2007; Connelly, 2004; Ashokan et al., 2003; Ashokan, 2008; Vyakaranam, 2012; Vyakaranam and Kokini, 2012; Vyakaranam, et al., 2012). Mixing in a Brabender Farinograph was explored numerically by Connelly (Connelly, 2004; Connelly and Kokini, 2004; Connelly and Kokini, 2006a, 2006b) using mesh superposition and particle tracking with a Newtonian fluid. The results were validated against laser Doppler anemometry (LDA) values obtained by Prakash and coworkers (Prakash, 1996; Prakash and Kokini, 1999, 2000; Prakash et al., 1999). Twin-screw mixers have also been simulated with more complex fluids. Successful simulation of mixing in a twin-screw mixer was performed using 2D finite element method (FEM) techniques; and these results were compared to those from previous 2D simulation of a single screw mixer (Connelly and Kokini, 2007). A generalized Newtonian Carreau fluid model was used in a mixed Galerkin FEM simulation.

Variation of mixing index with mixer operating conditions and configuration was not found to be significant (Cheng and Manas-Zloczower, 1997) but changing fluid rheology had an impact. The influence of rheology increased with non-Newtonian behavior (Prakash and Kokini, 1999). Viscoelasticity enlarged the areas of high mixing index, those with more elongational flow. Increased shear thinning caused greater areas of plug flow with low mixing index values. Shear stress was shifted in a viscoelastic fluid so that high shear stresses increased ahead of the blade and low shear stress moved behind the blade. Adding high values of shear stress to areas with elongational flow increased the dispersion ahead of the paddle. Conversely, increased shear stress magnitudes near the paddle tip increased the area of dead zones, thus hindering dispersion (Connelly and Kokini, 2004).

Recent work by Vyakaranam et al. (2012) has examined mixing in a Readco continuous mixer both experimentally and numerically. A high viscosity Newtonian corn syrup was used as the model fluid. Experimental measurements were made using LDA to determine fluid velocity and compared to values obtained via numerical simulation. Stagger angle of the mixer paddles caused local disruption but did not change global forward or reverse flow. Flow rate was found to be independent of stagger angle, but varied with screw speed. The axial component of velocity (v_z) was affected by stagger angle, but the horizontal component (v_x) and the vertical component (v_y) were unaffected.

2. Material and methods

2.1. Fluid rheology

This research focused on a non-Newtonian power-law fluid. Fluids that follow the power-law relation have a viscosity dependent on shear rate as found in the following equation:

$$\mathbf{T} = 2\eta(\dot{\gamma}, T)\mathbf{D} \tag{1}$$

where $\mathbf{T}$ is extra stress tensor, $\mathbf{D}$ is the rate of deformation tensor and η is dynamic viscosity, here a function of temperature T and local shear rate $\dot{\gamma}$ as seen below in Eq. (3). The extra stress tensor is isotropic and represents the effects of deformation on a material while being dependent on the gradient of fluid velocity and fluid

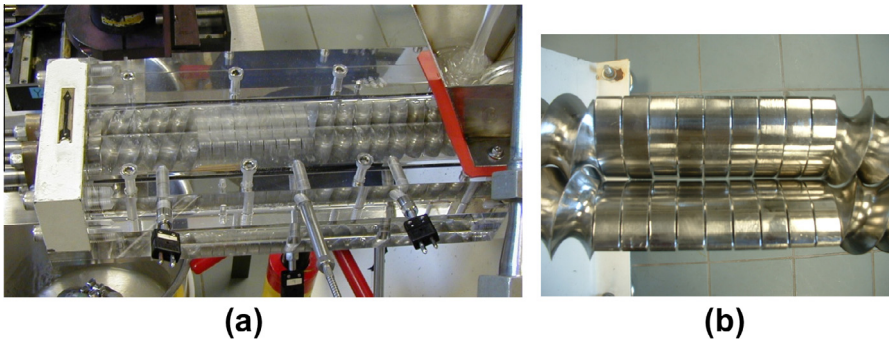

Fig. 1. (a) 2" Readco continuous processor with Plexiglas barrel and (b) close-up of paddles in parallel configuration (Ashokan, 2008).

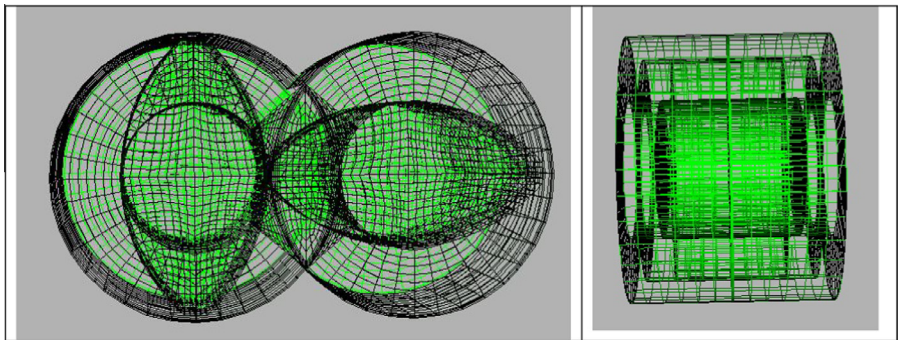

Fig. 2. 3D barrel mesh with two pairs of superimposed paddles (a) front view and (b) side view.

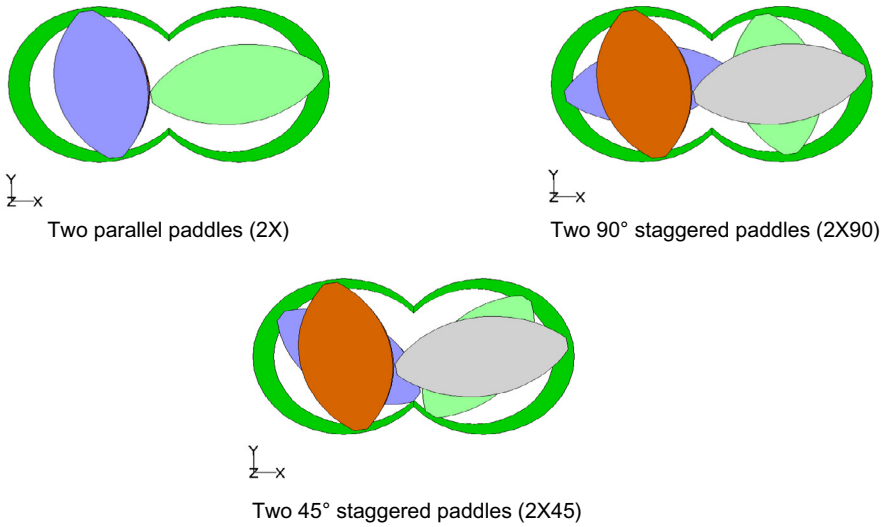

Fig. 3. Paddle angle used in simulations.

density. In the case of a Newtonian fluid, it is a linear function of the rate of deformation tensor:

$$\dot{\gamma} = \sqrt{2tr(\mathbf{D}^2)} \tag{2}$$

$$\eta = K(t\dot{\gamma})^{n-1} \tag{3}$$

where K is the consistency factor, t is the natural time, and n is the power-law index which is a property of the material.

A 2% by weight aqueous Carboxymethylcellulose (CMC) solution was modeled as a non-Newtonian power law fluid. CMC has served as a model fluid in much of our work to date (Prakash, 1996; Prakash and Kokini, 1999, 2000; Prakash et al., 1999; Connelly and Kokini, 2006a, 2006b; Fanning, 2009). The parameters for Eq. (3) were calculated by Prakash (1996) from steady shear measurement results as $K = 15.74$ N s^n m^2, $n = 0.397$, and $\lambda = 1$.

2.2. Characterization of mixing performance

Dispersive mixing was characterized by the Manas-Zloczower mixing index λ_{MZ} (Cheng and Manas-Zloczower, 1990):

$$\lambda_{MZ} = \frac{|\mathbf{D}|}{|\mathbf{D}| + |\mathbf{\Omega}|} \tag{4}$$

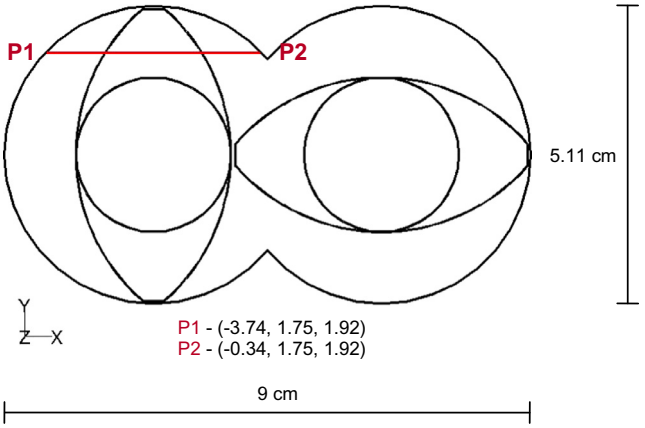

Fig. 4. Location of measurement points along the line between point P1 and point P2.

where **D** and **Ω** are the rate of deformation and vorticity tensors respectively. When $\lambda_{MZ} = 0$ it indicates pure rotational mixing, $\lambda_{MZ} = 0.5$ indicates simple shear flow, $\lambda_{MZ} = 0.7$ indicates efficient dispersive mixing, and $\lambda_{MZ} = 1$ indicates elongational flow. An additional measure to examine dispersive mixing is the distribution of shear stress (Manas-Zloczower and Kaufman, 2009).

2.3. Numerical simulations

Numerical simulations were performed using the Polyflow family of programs from ANSYS-Fluent, Inc. (Lebanon, NH). These are a CFD program suite including a mesh generator: Gambit, FEM solver: Polyflow, and graphics post-processor: CFX-Post. A Dell Precision 690 workstation with Dual Core Xeon processors and 16 GB RAM was used.

The boundary conditions used were no slip at the walls, fully developed Poiseuille flow in the region between paddles and barrel, and zero tangential velocity and normal force at the outflow. Isothermal flow was modeled with inertia taken into account, and gravity was neglected. Fluid parameters used were those for a 2% CMC solution described above with a density of 1.0068 g/cm^3. Viscosity and density values were measured at room temperature (23–25 °C). Mesh superposition was used to account for the moving paddles in the mixer geometry.

2.4. Mesh superposition

In order to account for the moving paddle elements without remeshing the entire fluid region for every time step, the mesh superposition technique was used. The paddles and barrel are meshed separately and then the paddles are superimposed on the barrel mesh. A barrel element is determined to be part of the solid paddle if more than 60% of it is overlapped by the paddle mesh. The threshold value was identified as that which gave good results in several different simulation problems performed by Polyflow. A value too small would not allow fluid flow between the screw and barrel wall and could allow a screw dimension which is larger than the barrel. Once a barrel element is considered part of the paddle as stated above, the velocity of that element is set equal to the velocity of the moving part. This adjustment is accomplished by the use of a penalty term $H(\mathbf{v} - \bar{\mathbf{v}})$ in the equation of motion as seen below in Eq. (5). H is a step function which equals 0 outside the moving part and 1 within it. The variable **v** is velocity; and $\bar{\mathbf{v}}$ is the local moving part velocity:

$$H(\mathbf{v} - \bar{\mathbf{v}}) + (1 - H)(-\nabla p + \nabla \cdot \mathbf{T} - \rho \mathbf{a}) = 0 \tag{5}$$

where p is the pressure, and $\rho\mathbf{a}$ is the acceleration term. Since gravity is neglected, there is no gravity term in Eq. (5).

The boundary between the solid and fluid elements can only be determined to within one element. When a small amount of fluid leakage into the paddle occurs (Jongen, 2000) a very small compression factor ($\beta = 0.01$) is added to the continuity equation to compensate for it and eliminate its effect on the computation. The modified equation then becomes as follows:

$$\nabla \cdot \mathbf{v} + \frac{\beta}{\eta} \nabla^2 p = 0 \tag{6}$$

2.5. Mixer geometry

The Readco continuous mixer (Fig. 1) model geometry was created and meshed for numerical simulation using Gambit (Fig. 2a and b). This mixer is a co-rotating mixer with initial and exiting conveying screws and nine pairs of self-wiping paddles in the cen-

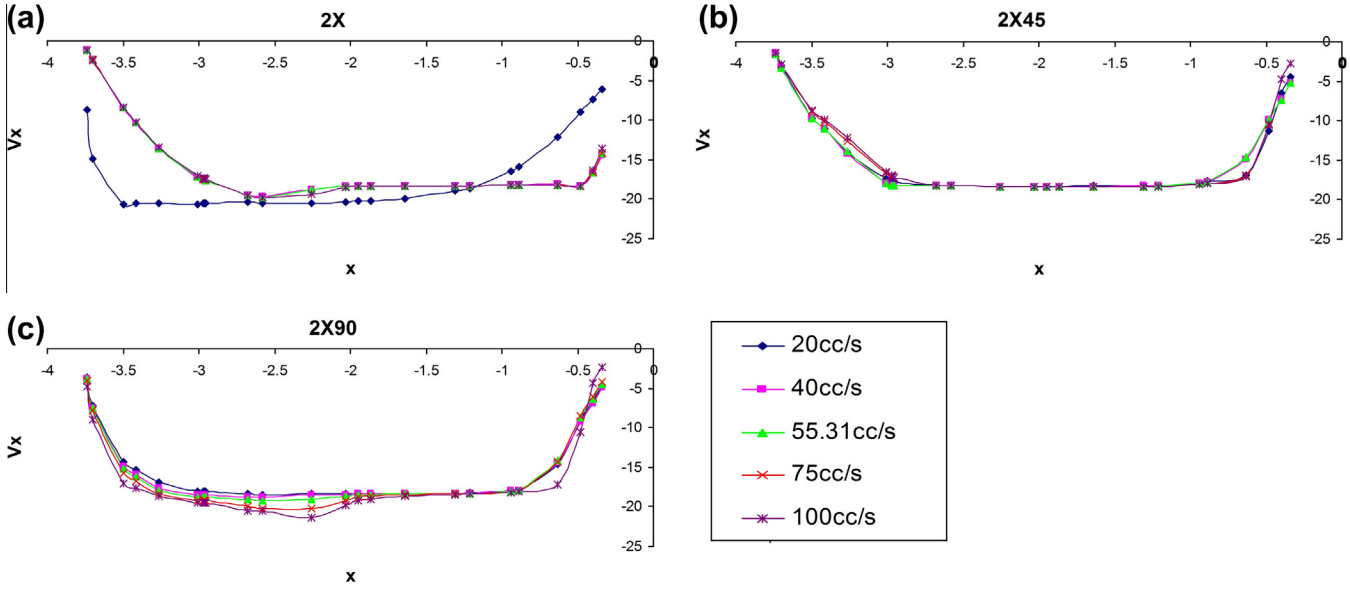

Fig. 5. X component of velocity different flow rates for 2×, 2 × 45, 2 × 90.

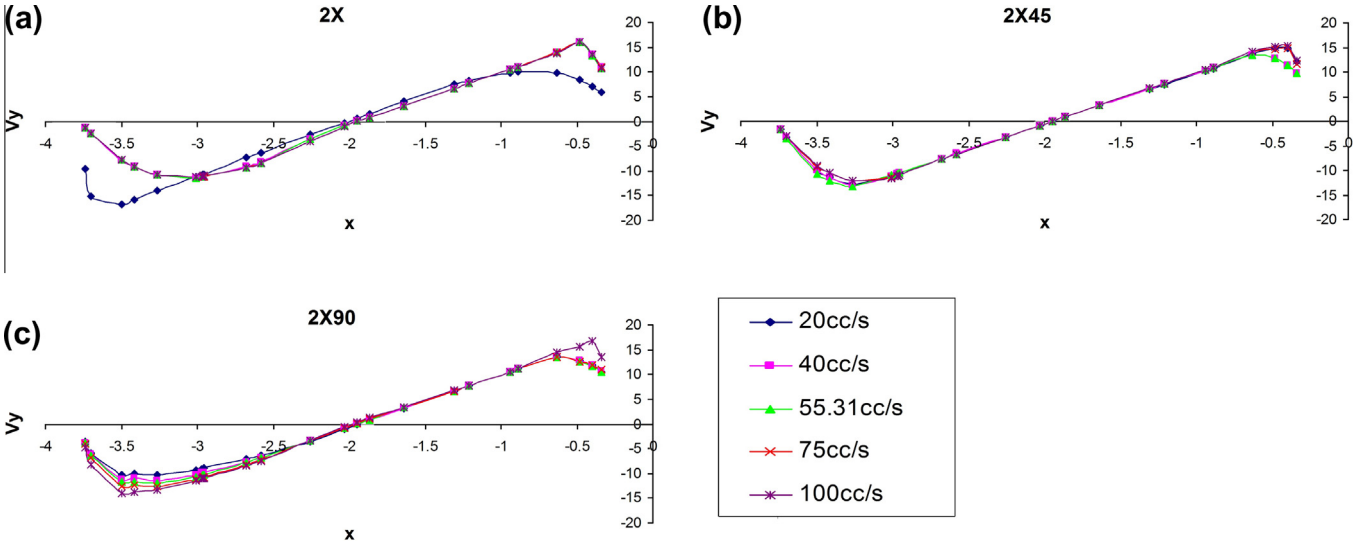

Fig. 6. Y component of velocity at different flow rates for 2×, 2 × 45, 2 × 90.

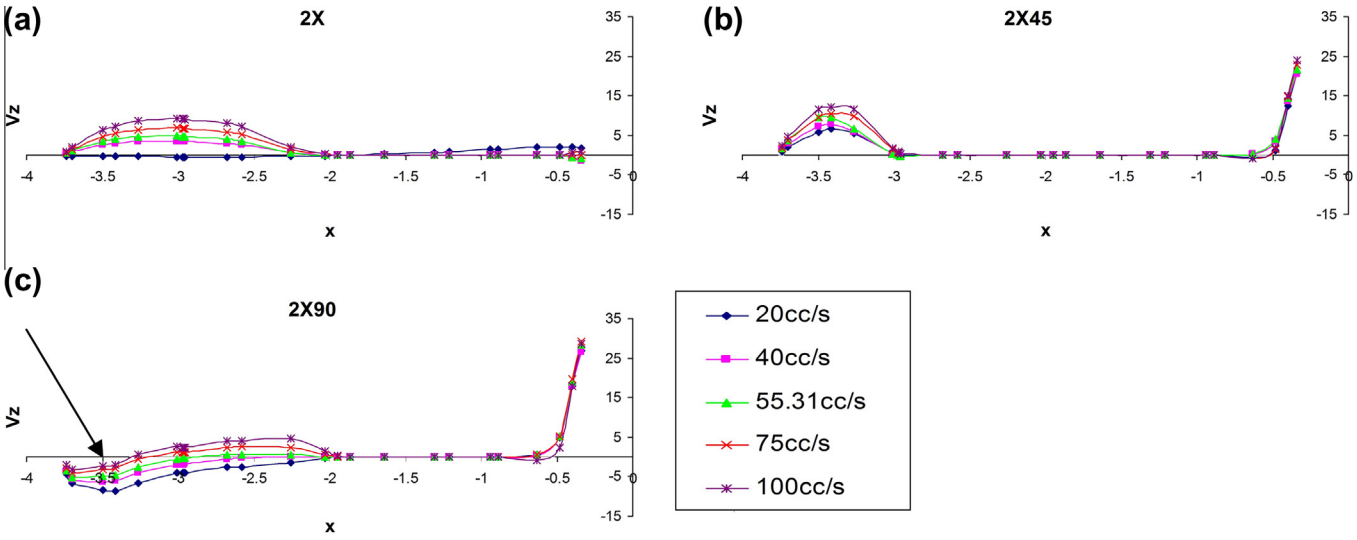

Fig. 7. Z component of velocity at different flow rates for 2×, 2 × 45, 2 × 90.

ter length of the mixer. Here only the mixing section of the mixer is examined. In order to balance computational cost with accuracy, several meshes with varying densities were developed and the resulting data was compared to experimental values. Root mean square differences were calculated for simulation velocities as a percent of the experimental values at several points in the mixer. Velocity magnitude data for the various meshes was also compared. This information was used to choose the best mesh combination for further simulations (Ashokan, 2008). The outcome was a choice of the least dense mesh which provided an accurate velocity profile and most closely coincided with experimental data. Further description of the method used can be found in Vyakaranam et al. (2012).

Paddle angles, rotation speeds, and fluid inflow rates were chosen based on the starting point (100 rpm and 55.31 cc/s) of previous experimental work in our laboratory (Fanning, 2009). Here, values were chosen above and below those used previously in experimental and simulation work to see the trend with changing mixer speed and fluid inflow rate. Paddles configurations were used with the second paddle set staggered at 0° (2×), 45° (2 × 45), and 90° (2 × 90) to the initial paddles. Mixer speeds of 50 rpm, 100 rpm, and 150 rpm were selected. Fluid inflow rates of 20 cc/s, 40 cc/s, 55.31 cc/s, 75 cc/s, and 100 cc/s were examined. Each simulation was run for one rotation of the paddles and results were recorded every 10°. Based on the mixer speed the output time at 10° is 0.033333 s at 50 rpm, 0.016667 s at 100 rpm, and 0.011111 s at 150 rpm.

The various paddle angles are shown below in Fig. 3. Fig. 4 below shows the line along which data points were taken. This line passes through the gap between the two paddle pairs. Velocities, shear rates, and mixing indices shown in the following graphs were obtained on the line between point P1 and point P2.

3. Results and discussion

3.1. Effect of flow rate on 3-D velocity distributions

Figs. 5–7 show v_x, v_y, and v_z plotted against x position along the line between points P1 and P2 for various flow rates. The horizon-

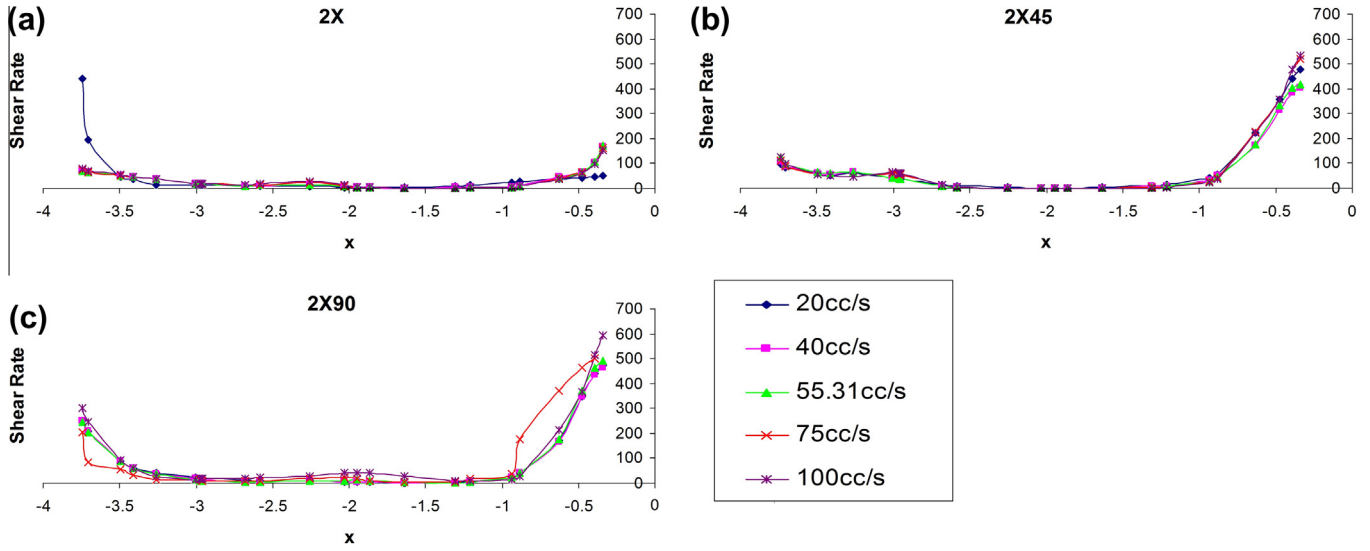

Fig. 8. Shear rate at different flow rates for 2×, 2 × 45, 2 × 90.

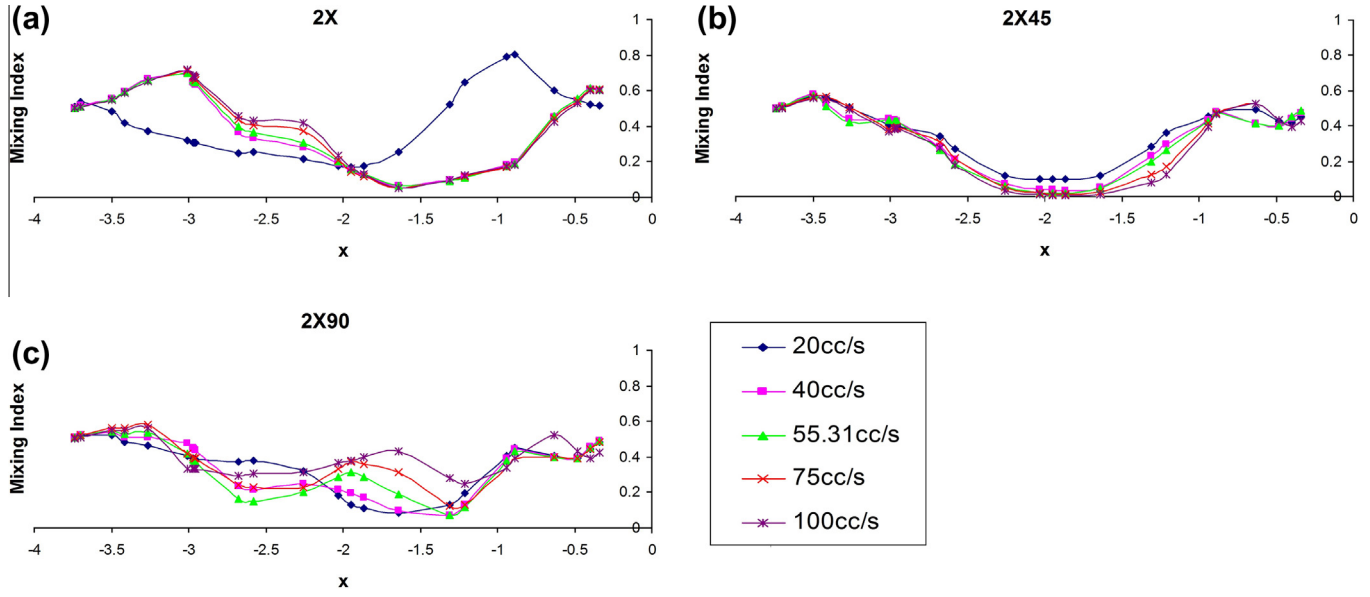

Fig. 9. Mixing index at different flow rates for 2×, 2 × 45, 2 × 90.

tal axis across the barrel is *x*, the vertical axis is *y*, and the axis from the inlet to the outlet of the mixer is *z*. The paddle angles are as shown in Fig. 3. Values of v_x have low magnitudes near the center of the mixer (*x* location closer to zero) and near the barrel wall (*x* location closer to −4). Negative values of v_y are seen near the barrel wall and positive values near the barrel center. These values are a logical result of the counterclockwise rotation of the paddles pushing the fluid up near the center of the mixer, across the top, and then down near the barrel wall.

There is no significant trend for v_x and v_y with increasing fluid flow rate in the 2× and 2 × 45 configurations (Figs. 5 and 6). The exception is 20 cc/s in the 2× configuration which is not a fast enough rate to follow the curves found with the other flow rates. Higher values near the barrel wall are generated because the lower fluid inflow rate allows the fluid in this area to spend more time in the mixer, experiencing more passes of the paddles. This effect does not occur in the fluid at the center of the mixer which is undergoing forward pumping motion advancing the fluid.

A characteristic critical flow rate does not appear in the staggered paddle configurations. The staggered paddles impart consistent v_x and v_y values to the fluid even at the lowest fluid inflow rate. In the 2 × 90 configuration (Figs. 5 and 6), increasing fluid inflow rate increases the magnitude of negative v_x and v_y values as the fluid approaches the barrel wall where faster fluid flow aids in increased mixing, adding to the fluid motion caused by the paddles. Increasing flow rate increases v_z. At a constant flow rate, average v_z would be constant in a pipe. Average v_z should also be constant at a constant flow rate in a complex geometry, but it is not. Our observation of increasing v_z is counter-intuitive and unexpected. Constant flow should produce constant v_z in steady state flow, but here it does not due to the complexity of the geometry.

Increasing stagger angle increases v_z near the center of the mixer, resulting in more flow-through in this area. Increased v_z with staggered paddles is unexpected because staggered paddle configurations are frequently chosen to increase mixing and fluid reorientation. Staggered paddles are generally expected to decrease v_z

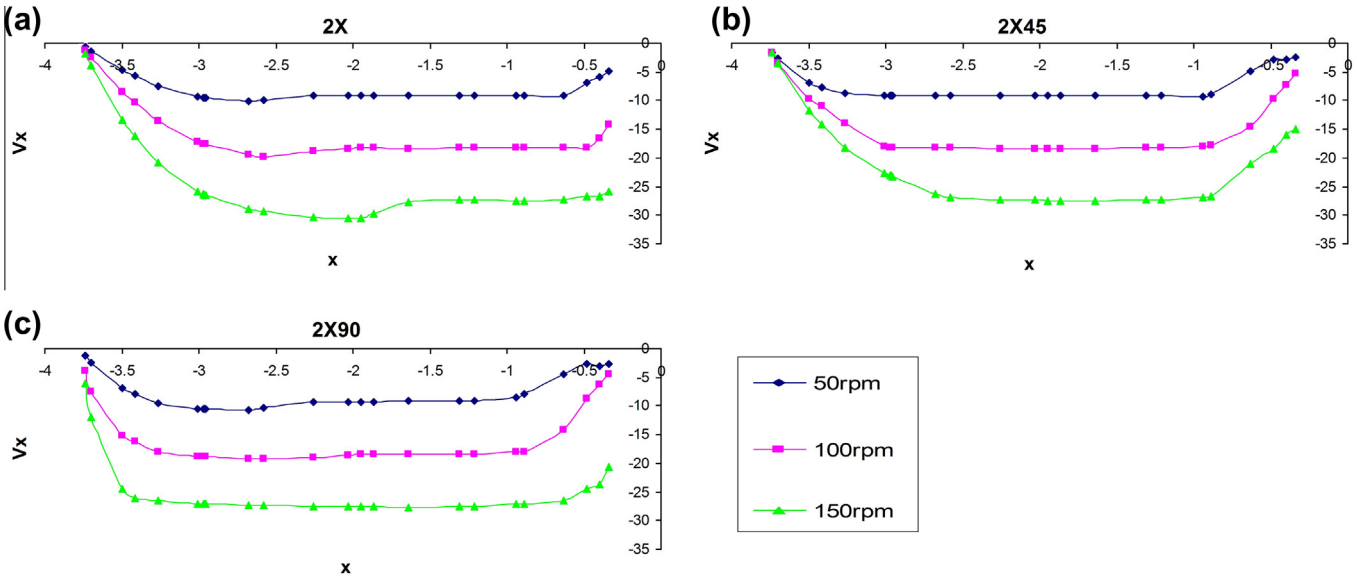

Fig. 10. X velocity component at different rotation speeds for 2×, 2 × 45, 2 × 90.

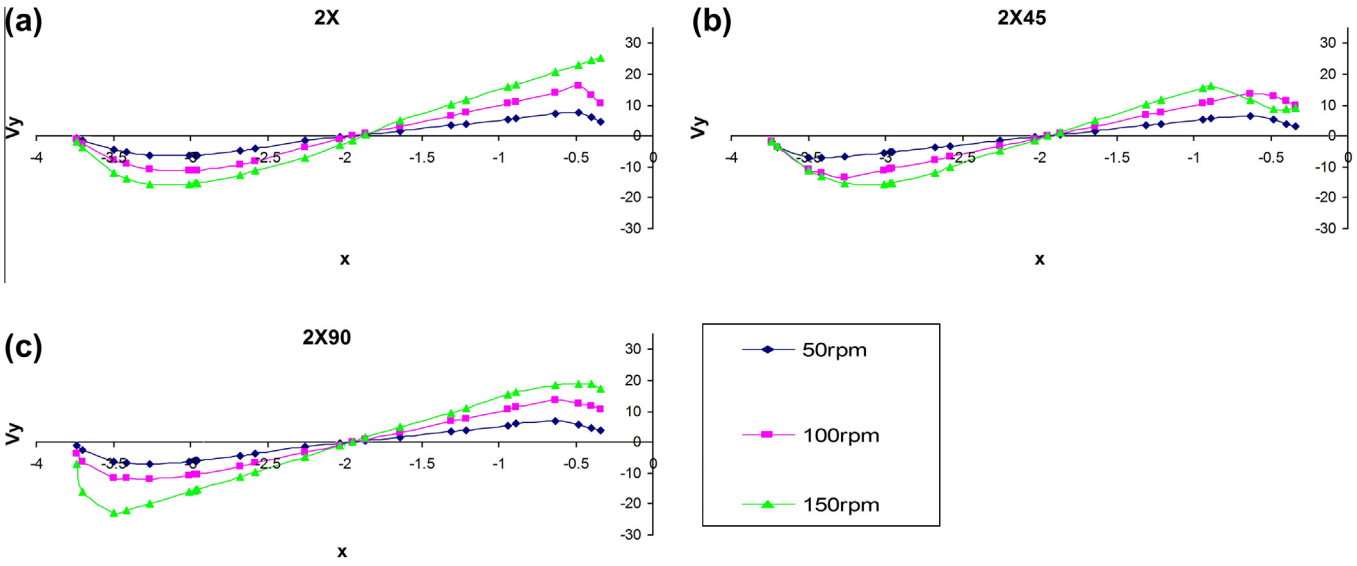

Fig. 11. Y velocity component at different rotation speeds for 2×, 2 × 45, 2 × 90.

and possibly generate areas of backflow like those seen in the 2 × 90 configuration (Fig. 7c). Backflow is indicated by negative v_z and marked by an arrow in the figure. The additional conveying effect in the center of the mixer, due to the influence of both the left and right-hand paddles, is enhanced by the staggered paddles.

3.2. Effect of flow rate on shear rate and mixing index

Shear rate values are higher near the center of the mixer for staggered configurations (Fig. 8). Maximum shear rate for both staggered geometries is significantly larger than that found for 2×; and the peak for 2 × 90 is greater than that for 2 × 45. The higher shear rate near the center of the mixer is found because the fluid passes in a narrow space between two objects moving in the opposite direction. A higher shear rate is also found where the fluid is forced between the paddle and barrel wall because of the narrow space. In this area, only one object is moving so the values are smaller than those in the center. Increasing flow rate did not significantly affect shear rate values. The exception, once again, is the 20 cc/s rate in the 2× geometry. This flow is below the critical rate necessary to mirror the trend seen at the other values.

Increasing flow rate increases the elongational contribution to the mixing index (Fig. 9). This faster flow minimizes the rotational impact on the fluid as it spends less time in the mixer and is moved primarily in the axial direction through the mixer. Again the fluid inflow rate of 20 cc/s is below the critical value needed in the 2× configuration to follow the trend seen at higher flow rates. In particular, there is an area of efficient dispersive mixing ($\lambda_{MZ} = 0.7$) between the paddle center and the barrel wall for all flow rates greater than 20 cc/s.

Simple shear flow ($\lambda_{MZ} = 0.5$) occurs near the barrel wall and center which coincides with the higher shear rate values seen above. Most rotational flow occurs at mid-range x values, near the center axis of the paddle due to the location of these points

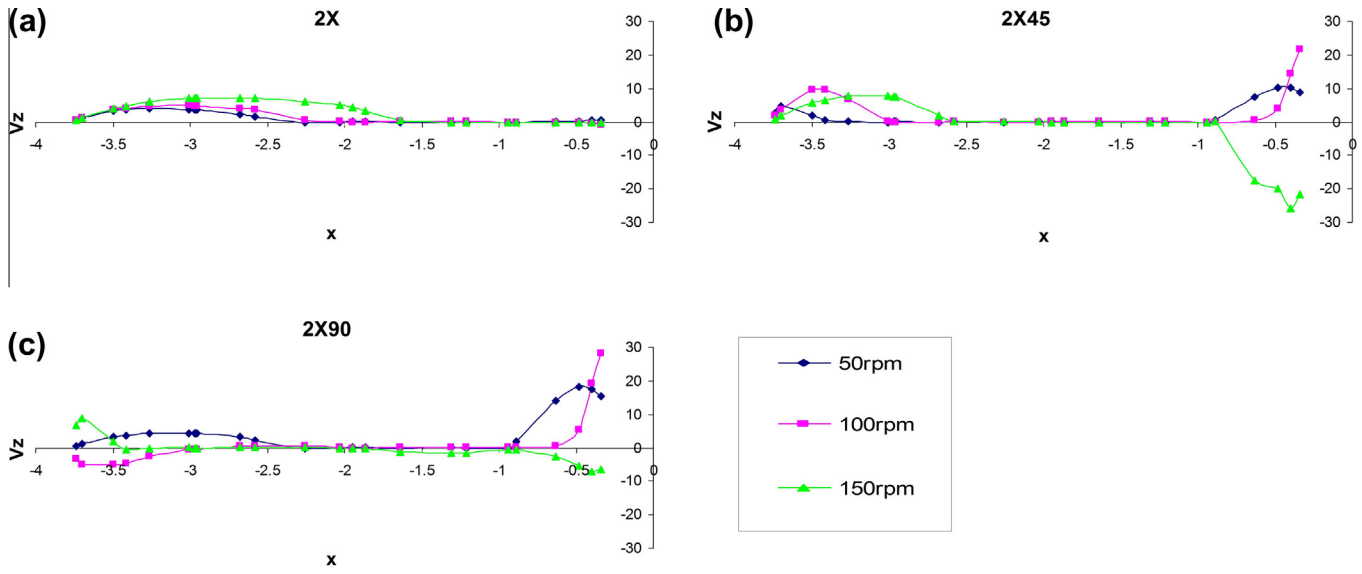

Fig. 12. Z velocity component at different rotation speeds for 2×, 2 × 45, 2 × 90.

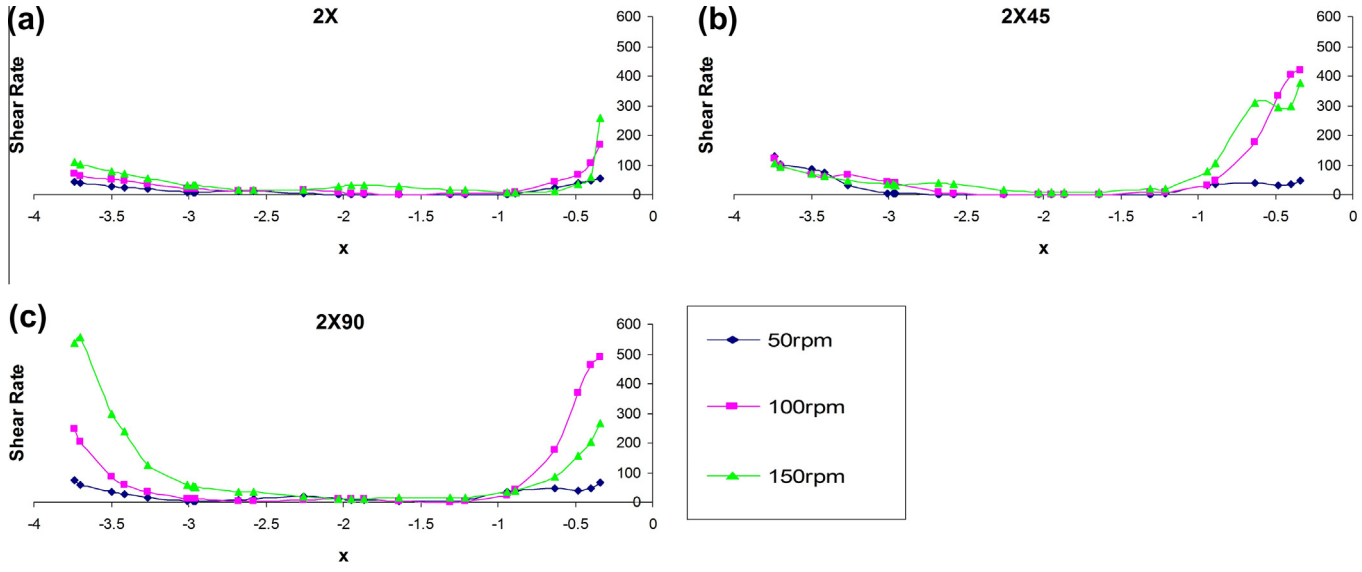

Fig. 13. Shear rate at different rotation speeds for 2×, 2 × 45, 2 × 90.

with respect to the hub of rotation. In Fig. 9b, the 2 × 45 configuration shows a neat pattern of mixing index values with shear flow near the center of the mixer and the barrel wall and pure rotational flow ($\lambda_{MZ} = 0$) in the center of the paddle. Both 2× and 2 × 90 have additional fluid disruption and have no areas of pure rotational flow.

3.3. Effect of mixer speed on 3D velocity distribution

Increasing mixer speed increased $\boldsymbol{v_x}$ magnitude (Fig. 10) but the trend remains the same with stagger angle. There is little variation between 2×, 2 × 45, and 2 × 90. Only the number of points at maximum velocity magnitude increases with increasing stagger angle. The largest magnitude velocity values for each mixer speed are the same for all three geometries. In Fig. 11, $\boldsymbol{v_y}$ has negative values near the barrel wall and positive values near the barrel center. Increasing $\boldsymbol{v_y}$ magnitude occurs with increasing mixer speed. Trends seen for $\boldsymbol{v_x}$ and $\boldsymbol{v_y}$ coincide with the fluid motion in the mixer. The paddle pushes fluid up near the center of the mixer, across the top, and down near the barrel wall due to the counter-clockwise rotation. The three configurations have very similar trends for all mixer speeds.

Increasing mixer speed increases $\boldsymbol{v_z}$ in the 2× geometry (Fig. 12). This trend does not continue in the staggered configurations. In fact, areas of backflow are seen in both 2 × 45 and 2 × 90 at 150 rpm. Backflow causes fluid to spend more time in the mixer instead of flowing directly through it enabling the mixer to cause more reorientation.

3.4. Effect of mixer speed on shear rate and mixing index

Shear rate values increase with increasing mixer speed near the barrel wall of the mixer (Fig. 13) corresponding with the squeezing of the fluid between the paddle tip and barrel wall as the paddle rotates. In the center of the mixer, the fluid also experiences shearing forces due to the movement of both paddle sets.

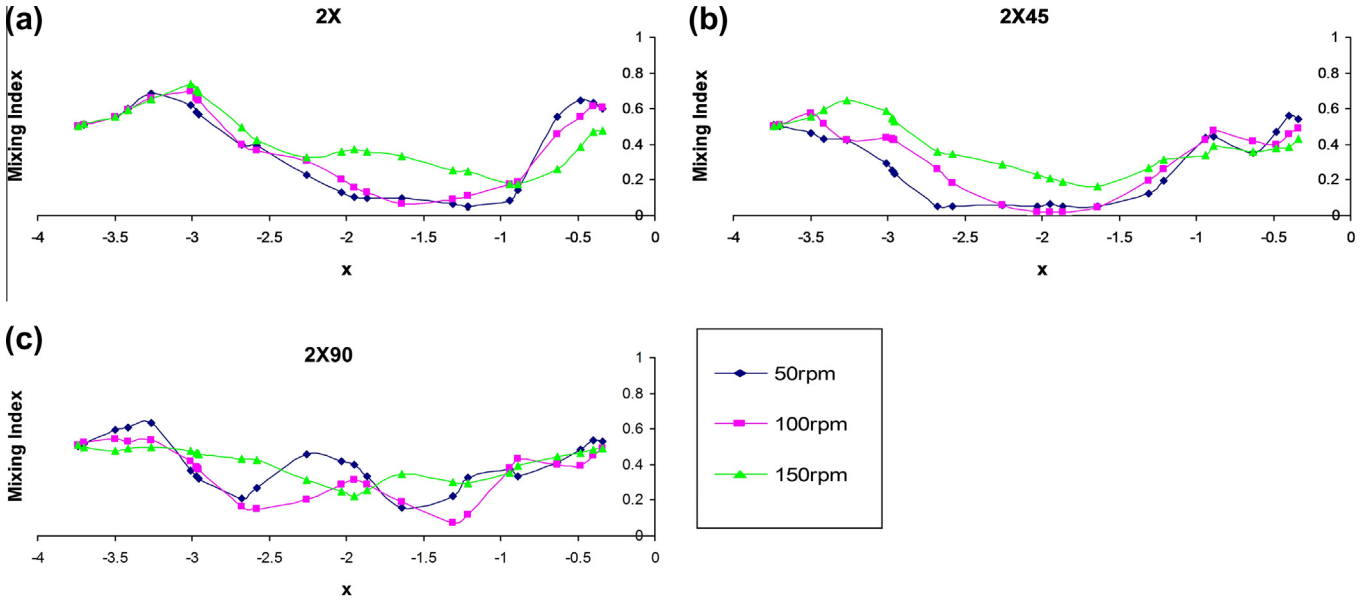

Fig. 14. Mixing index at different rotation speeds for 2×, 2 × 45, 2 × 90.

Due to the 90° angle between the right and left-hand paddle, each imparts opposing motion to the fluid. Near the barrel center, increasing the mixer speed from 50 rpm to 100 rpm increases shear rate and increasing the mixer speed from 100 rpm to 150 rpm decreases the shear rate. The highest speed seems to indicate a speed above which further increases in mixer speed do not positively affect shear rate. Both staggered configurations have higher maximum shear rates than 2×, but 2 × 90 has the highest peak. This peak is seen near the mixer center at 100 rpm and moves to the barrel wall at 150 rpm, indicating a change in shear flow location at higher speed.

Increasing the mixer speed increases the mixing index near the barrel wall in the 2× and 2 × 45 configurations (Fig. 14). Simple shear flow ($\lambda_{MZ} = 0.5$) is seen in areas of high shear rate noted above. Higher mixing index values indicate more elongational flow which is surprising given that increasing the mixer speed should increase the rotational flow. The converse is true near the barrel center and throughout the 2 × 90 configuration. This result coincides with the expectation that increased rotation speed increases the rotational contribution to the mixing index.

4. Conclusions

Increasing mixer speed increases v_x and v_y values, indicating more mixing, while increasing fluid inflow rate increases v_z values, indicating greater flow-through. In relation, increasing fluid inflow rate increases elongational contribution to the mixing index. Additionally, increasing paddle stagger angle increases v_z near the barrel center and maximum shear rate value.

High mixing index values combined with high shear rates are necessary to break most agglomerates. The 2 × 90 paddle configuration operating at 100 rpm with a fluid inflow rate of 100 cc/s shows the highest shear rate. Although 2 × 90 shows several values indicating simple shear flow, the 2× paddle configuration indicates efficient dispersive mixing with $\lambda_{MZ} = 0.7$ at flow rates greater than 20 cc/s. Thus 2× is the best paddle configuration to promote efficient dispersive mixing. Examining the 2 × 90 trend, perhaps increasing the fluid inflow rate would increase the efficiency of dispersive mixing in this configuration.

This research explored a simplified mixer and observed the effect of paddle angle and operating conditions. Backward staggered paddles are expected to enhance mixing. It would be informative to see the effect compared with the forward staggered data shown here. In this work, dispersive mixing is examined. It would be fruitful to investigate distributive mixing as well since this also contributes to the overall quality of the final product.

References

Alsteens, B., Legat, V., Avalosse, T., 2004. Parametric study of the mixing efficiency in a kneading block section of a twin-screw extruder. International Polymer Processing 19, 207.

Alvarez, M.M., Zalc, J.M., Shinbrot, T., Arratia, P.E., Muzzio, F.J., 2002. Mechanisms of mixing and creation of structure in laminar stirred tanks. AIChE Journal 8 (10), 2135.

Ashokan, B.K., 2008. Developing Methods for Design of Continuous Mixers Through 3D Numerical Simulation of Flow and Mixing. PhD Thesis. Department of Food Science, Rutgers University, New Brunswick.

Ashokan, B.K., Fanning, L., Connelly, R.K., Kokini, J.L., 2003. Determination of the flow and mixing in a continuous mixer using LDA and 3D simulation. In: Proceedings of the Eighth Conference of Food Engineering, A Topical Conference Held in Conjunction with the 2003 AIChE Annual Meeting, San Francisco, CA.

Cheng, J.J., Manas-Zloczower, I., 1990. Flow field characterization in a Banbury mixer. International Polymer Processing 5 (3), 178.

Cheng, H., Manas-Zloczower, I., 1997. Study of mixing efficiency in kneading discs of co-rotating twin-screw extruders. Polymer Science and Engineering 37 (6), 1082.

Connelly, R.K., 2004. Numerical Simulation and Validation of the Mixing of Dough-Like Materials in Model Batch and Continuous Dough Mixers. PhD Thesis. Department of Food Science, Rutgers University, New Brunswick.

Connelly, R.K., Kokini, J.L., 2003. 2-D numerical simulation of differential viscoelastic fluids in a single-screw continuous mixer: application of viscoelastic finite element methods. Advances in Polymer Technology 22 (1), 22.

Connelly, R.K., Kokini, J.L., 2004. The effect of shear thinning and differential viscoelasticity on mixing in a model 2D mixer as determined using FEM with particle tracking. Journal of Non-Newtonian Fluid Mechanics 123 (1), 1.

Connelly, R.K., Kokini, J.L., 2006a. 3D numerical simulation of the flow of viscous Newtonian and shear thinning fluids in a twin sigma blade mixer. Advances in Polymer Technology 25 (3), 182.

Connelly, R.K., Kokini, J.L., 2006b. Mixing simulation of a viscous Newtonian liquid in a twin sigma blade mixer. AIChE Journal 52 (10), 3383.

Connelly, R.K., Kokini, J.L., 2007. Examination of the mixing ability of single and twin screw mixers using 2D finite element method simulation with particle tracking. Journal of Food Engineering 79 (3), 956.

Fanning, L., 2009. Characterization of Velocity and Shear Rate Distribution in a Continuous Mixer. MS Thesis. Department of Food Science, Rutgers University, New Brunswick, NJ.

Jongen, T., 2000. Characterization of batch mixers using numerical flow simulations. AIChE Journal 46 (11), 2140.
Lamberto, D.J., Alvarez, M.M., Muzzio, F.J., 2001. Computational analysis of regular and chaotic mixing in a stirred tank reactor. Chemical Engineering Science 56, 4887.
Manas-Zloczower, I., Kaufman, M., 2009. Mixing measures. In: Manas-Zloczower, I. (Ed.), Mixing and Compounding of Polymers: Theory and Practice. Karl Hanser Verlag, Munich, p. 252.
Portillo, P.M., Ierapetritou, M.G., Muzzio, F.J., 2008. Characterization of continuous convective powder mixing processes. Powder Technology 182, 368.
Portillo, P.M., Ierapetritou, M.G., Muzzio, F.J., 2009. Effects of rotation rate, mixing angle, and cohesion in two continuous powder mixers—a statistical approach. Powder Technology 194, 217.
Prakash, S., 1996. Characterization of Shear Rate Distribution in a Model Mixer Using Laser Doppler Anemometry. PhD Thesis. Department of Food Science, Rutgers University, New Brunswick.
Prakash, S., Kokini, J.L., 1999. Determination of mixing efficiency in a model food mixer. Advances in Polymer Technology 18 (3), 209.
Prakash, S., Kokini, J.L., 2000. Estimation and prediction of shear rate distribution as a model mixer. Journal of Food Engineering 44 (3), 135.
Prakash, S., Karwe, M., Kokini, J.L., 1999. Measurement of velocity distribution in the Brabender Farinograph as a model mixer, using laser-Doppler anemometry. Journal of Food Process Engineering 22 (6), 435.
Vyakaranam, K.V., 2012. Analysis of dispersive mixing and breakup of air bubbles during continuous mixing of viscous liquids using experimental and numerical simulation techniques. PhD Thesis. Department of Food Science, Rutgers University, New Brunswick.
Vyakaranam, K.V., Kokini, J.L., 2012. Prediction of air bubble dispersion in a viscous fluid in twin screw continuous mixer using FEM simulations of dispersive mixing. Chemical Engineering Science 84, 303.
Vyakaranam, K.V., Ashokan, B.K., Kokini, J.L., 2012. Evaluation of effect of paddle element stagger angle on the local velocity profiles in a twin-screw continuous mixer with viscous flow using finite element method simulations. Journal of Food Engineering 108 (4), 585.
Zalc, J.M., Alvarez, M.M., Muzzio, F.J., Arik, B.E., 2001. Extensive validation of laminar flow in a stirred tank with three Rushton turbines. AIChE Journal 47 (10), 2144.
Zhang, X.M., Feng, L.F., Chen, W.X., Hu, G.H., 2009. Numerical simulation and experimental validation of mixing performance of kneading discs in a twin screw extruder. Polymer Engineering and Science 49 (9), 1772.